

## Tuning nanopatterns on fused silica substrates: a theoretical and experimental approach†

Rodica Morarescu,<sup>\*a</sup> Lars Englert,<sup>b</sup> Branko Kolaric,<sup>a</sup> Pascal Damman,<sup>a</sup> Renaud A. L. Vallée,<sup>c</sup> Thomas Baumert,<sup>b</sup> Frank Hubenthal<sup>b</sup> and Frank Träger<sup>b</sup>

Received 8th November 2010, Accepted 7th February 2011

DOI: 10.1039/c0jm03829f

In this study we develop a novel approach to tune nanopatterns on fused silica substrates exploiting the polarization dependence of the strongly localized near field of highly ordered triangular nanoparticle arrays. For this purpose such arrays were prepared by nanosphere lithography on fused silica substrates and subsequently irradiated with single 35 fs long laser pulses. The irradiation leads to the excitation of localized surface plasmon polariton resonances, followed by ablation of the nanoparticles and partially of the substrate. By this means, nanostructures were generated on the substrate surface, reflecting the local fields in the vicinity of the triangular nanoparticles. Depending on the applied fluence, small holes as well as extended nanostructures with dimensions well below the diffraction limit have been created. Furthermore, by rotating the linear polarization of the laser light by 90° with respect to the orientation of triangular nanoparticles, different plasmon modes have been excited, which in turn, alter the local field distribution. As a result, either nanochannels or bone like shaped nanogrooves in a chequered structure were generated on the fused silica substrates. Finite-difference time-domain simulations demonstrate, that the results can, in fact, be explained by the enhanced near field distribution, which is dominated by the excitation of localized surface plasmon polariton resonances in the triangular nanoparticles. It is shown, that the fluence and the polarization of the laser light are the key parameters in nanogroove and nanochannel formation.

### I. Introduction

In nanotechnology, the generation of nanopatterns with complex morphologies having dimensions well below the optical diffraction

limit remains an ambitious challenge. Behind the fundamental interest in understanding the physical process of morphogenesis at a surface, the motivation to study nanopatterning is also driven by the great potential of such nanostructures for advanced applications in *e.g.* nanofluidics, nanophotonics and biomedical devices.<sup>1–3</sup>

Nowadays numerous methods are able to generate nanopatterns *e.g.* combining different physical stresses (electric, magnetic, thermal, elastic) conventional top-down lithography techniques or laser induced surface structuring. The latter method is a method of choice that allows the precise generation of nanopatterns with dimensions below the optical diffraction limit.<sup>4</sup> One approach to achieve such nanostructures is to exploit the near field of a microscope tip illuminated with laser light,<sup>5</sup> although this technique is not suitable for many applications due to its limited throughput. A more promising approach, which has attracted increasingly more attention in recent years, exploits the near field of latex or SiO<sub>2</sub> micro- and nanosphere arrays on substrates, irradiated with ns- or fs-pulsed laser light.<sup>6,7</sup> Due to the lens effect of the spheres, high electromagnetic fields in the vicinity of the substrate are generated, which overcome the ablation threshold.<sup>8,9</sup> Depending on the arrangement of the spheres, highly ordered arrays of nanoholes are created in the substrate.<sup>10</sup> Recently similar experiments were undertaken using spherical noble metal particles, exploiting their unique optical properties, which are dominated by the excitation of localized surface plasmon polariton resonances (LSPPRs). These collective oscillations of the conduction band electrons are accompanied by an enhancement of the local field in the vicinity of the nanoparticle (NP) surface. This enhanced local field in combination with the focusing effect due to the sphere itself, allows generation of distinct types of nanopatterns.<sup>11,13–15</sup> It was shown that when gold nanospheres with a diameter of approximately 200 nm are illuminated with linearly polarized fs-pulsed laser light, the local field distribution underneath the NP creates elongated holes<sup>13</sup> oriented along the polarization direction. Motivated by these results, great attention has been paid to nonspherical NPs, which generate much stronger and more sophisticated local electromagnetic fields.<sup>16</sup> In particular, NPs with sharp tips, such as triangular nanoprisms show a great potential to generate well defined nanoscale structures over large areas of the substrate.<sup>17</sup>

In this paper we demonstrate an innovative and inexpensive method for tuning nanopatterns with dimensions well below the diffraction limit on fused silica substrates. The method is based on local ablation of the substrate surface due to the electromagnetic field

<sup>a</sup>Laboratoire Interfaces & Fluides Complexes, Centre d'Innovation et de Recherche en Matériaux Polymères, Université de Mons, 20 Place du Parc, B-7000 Mons, Belgium. E-mail: rodica.morarescu@umons.ac.be

<sup>b</sup>Institut für Physik and Center for Interdisciplinary Nanostructure Science and Technology (CINSaT), Universität Kassel, Heinrich-Plett-Str. 40, 34132 Kassel, Germany

<sup>c</sup>Centre de Recherche Paul Pascal (CNRS-UPR8641), 115 avenue du docteur Schweitzer, 33600 Pessac, France

† Electronic supplementary information (ESI) available: Experimental information and additional characterisation. See DOI: 10.1039/c0jm03829f

enhancements in the vicinity of highly ordered triangular gold NPs. Large surface areas can be patterned with well-defined nanostructures, by applying single 35 fs laser pulses to the sample. The advantage of this approach lies in its versatility: for a given geometry of the highly ordered NP arrays, several nanopatterns can be generated by ablation controlling the applied fluence and, more importantly the polarization direction of the laser light with respect to the NP orientation. To explain the morphology of the generated nanostructures, finite-difference time-domain simulations (FDTD) have been performed. The simulations show, that the generated nanostructures can indeed be explained by the local field enhancements. These structures are expected to play a major role in technological applications, such as biochemical chips and waveguides.<sup>18,19</sup>

Experiments presented here use arrays of triangular gold NPs prepared by nanosphere lithography,<sup>20</sup> utilizing the drop coating method of Micheletto *et al.*<sup>21</sup> Subsequently the samples were irradiated under ambient conditions with a single femtosecond light pulse, generated by an amplified Ti : sapphire laser system, coupled to a modified microscope set-up. The pulse duration was 35 fs full width at half maximum and the diameter of the laser spot on the sample was set to 22  $\mu\text{m}$ . The NP arrays were irradiated using linear or circular polarized light under normal incidence with a central wavelength of  $\lambda \approx 790$  nm. In order to increase the energy range, the pulse energy has been varied from  $E = 0.1$   $\mu\text{J}$  to  $E = 7.0$   $\mu\text{J}$ . The NPs have an aspect ratio (AR) of 2.47 (edge length divided by the NP height). The extinction spectrum of the NPs (see ESI†) exhibits a strong plasmon resonance at  $\lambda = 730$  nm due to the excitation of the dipolar mode.<sup>22–24</sup> Hence, the chosen wavelength of the laser light, at  $\lambda \approx 790$  nm, strongly excites this mode of the triangular gold NPs. The NPs as well as the imprinted nanopatterns have been characterized by atomic force microscopy (AFM), scanning electron microscopy (SEM), and extinction spectroscopy. A detailed description of the experimental procedure, samples characterization, experimental set-up and FDTD simulations respectively is presented in the Electronic Supplementary Information†.

## II. Results and discussion

A broad range of laser fluences have been studied in single shot experiments, exploiting the Gaussian intensity distribution of the incident laser light. Along these lines, four different regions have been identified. We emphasize, that the triangular gold NPs have been

completely removed from the substrate after a single pulse. According to our definition, the applied fluence is low, medium, high, and beyond the ablation threshold in regions 1, 2, 3, and 4, respectively. While in regions 1 to 3, well-defined nanopatterns appear, the fluence in region 4 is so high, that an unstructured ablation occurs. The definition of these 4 regions is justified, because similar local fluences on the surface irradiating spot result in similar structures, independent of the applied energy. The only difference is, that the regions 1 to 3 appear further away from the spot center for increasing energy and region 4 increases in diameter for higher energies. In the following, we present different generated nanostructures and show that these structures are the result of the localization of the electromagnetic field due to excitation of plasmon resonances in the triangular NPs. For an appropriately chosen energy, the ablation threshold of the substrate is surmounted exclusively in tiny areas in close vicinity of the triangular NPs.

### A. Influence of the Gaussian intensity distribution on nanopattern formation

In first experiments the influence of the applied energy on the morphology of the generated nanopattern was investigated. For this purpose, the Gaussian energy distribution of the intensity profile within the laser spot was exploited. The energy was set to  $E = 0.16$   $\mu\text{J}$  and the incident polarization direction was almost parallel to the bisectors of the triangles. Fig. 1a–c show AFM images of fused silica surfaces after irradiation, obtained in regions 1, 2, and 3. Although the illuminated area had a diameter of 22  $\mu\text{m}$ , only in an area with a diameter of 16  $\mu\text{m}$  are nanostructures created. The reason is, that outside this region even the enhanced local field in the vicinity of the NPs does not overcome the ablation threshold of fused silica ( $\sim 2$   $\text{J cm}^{-2}$ ).<sup>25,26</sup> In region 1, where the approximate local fluence was  $0.056$   $\text{J cm}^{-2}$  small elliptical holes are generated (Fig. 1a). In region 2 (local fluence  $\approx 0.072$   $\text{J cm}^{-2}$ ) nanostructures composed of three clearly distinct holes are created, one of them being large and two others being small (Fig. 1b). Finally, for high fluence (region 3, the local fluence  $\approx 0.082$   $\text{J cm}^{-2}$ ) the holes are completely merged and form nanogrooves with a bone-like shape in a chequered structure (Fig. 1c). The morphological details of the different nanostructures are summarized in Table 1. The results clearly demonstrate, that even the largest generated nanostructures have dimensions well below the diffraction limit. We emphasize, that minor shape variations of the nanostructures are mainly due to the strong Gaussian intensity

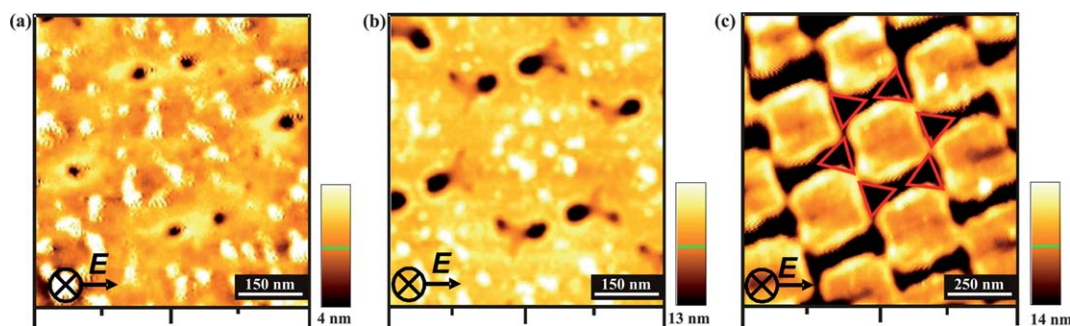


**Fig. 1** AFM images of the generated nanopatterns in region 1 (a), region 2 (b), and region 3 (c). The applied pulse energy was  $E = 0.16$   $\mu\text{J}$ . The red triangles indicate the original position of the triangular NPs on the substrate prior to irradiation. For clarity reasons, the red triangles have been drawn larger than the original NPs, which, in fact, have a tip to tip distance of approximately 100 nm. The black arrows indicate the polarization direction of the incoming laser light.

**Table 1** Characteristic features of the generated nanostructures for different fluences. The polarization of the applied laser light was parallel to the common bisector of two neighboring NPs, (*cf.* Fig. 1)

| Region | Average local fluence/ $J\text{ cm}^{-2}$ | Structure      | Average depth/nm | Average length/nm | Average width/nm |
|--------|---|----------------|------------------|-------------------|------------------|
| 1      | 0.056                                     | Holes          | $4.5 \pm 0.5$    | $23 \pm 3$        | $23 \pm 3$       |
| 2      | 0.072                                     | Large subholes | $13 \pm 2$       | $45 \pm 5$        | $34 \pm 4$       |
|        |   | Small subholes | $4.5 \pm 1.5$    | $23 \pm 2$        | $23 \pm 2$       |
| 3      | 0.082                                     | Nanogrooves    | $14 \pm 2$       | $287 \pm 10$      | $44 \pm 8$       |

distribution of the laser spot. As shown in our previous publication,<sup>17</sup> a homogeneous intensity distribution, *i.e.*, a larger spot diameter, results in nanopatterns of high uniformity. For an easy interpretation of the morphology of the generated nanostructures, the initial position of the triangular NPs (red triangles) and the polarization direction (black  $E$ -field vector) of the laser light are indicated in Fig. 1. Although the average fluence of the laser light is below the ablation threshold in regions 1 to 3, ablation occurs. This can be explained by the strong localization and enhancement of the fields in the vicinity of the NPs. The general trend, that larger structures appear closer to the center of the laser spot, can be easily explained by the Gaussian energy distribution of the laser beam. At the edge of the laser spot, the fluence is relatively low and no or only minor ablation occurs. In contrast, close to the center (region 3), the fluence increases, more material is ablated and larger nanostructures appear. We emphasize, that all created nanostructures are located at the original positions of the removed triangular NPs and the distance between the structures corresponds to the diameter of the nanospheres used for the lithographic mask.

To confirm the origin of the generated nanostructures, FDTD simulations have been performed. Fig. 2 illustrates the electric field energy density distribution for a polarization direction parallel to the bisector of the triangular NPs. In this case, the largest fields are generated only on the tip that points in the polarization direction. The two tips oriented perpendicular to this direction exhibit only small field enhancements. These calculations explain the origin of the observed experimental results presented in Fig. 1. For a low applied fluence, only at the tips exhibiting the largest field enhancements, the

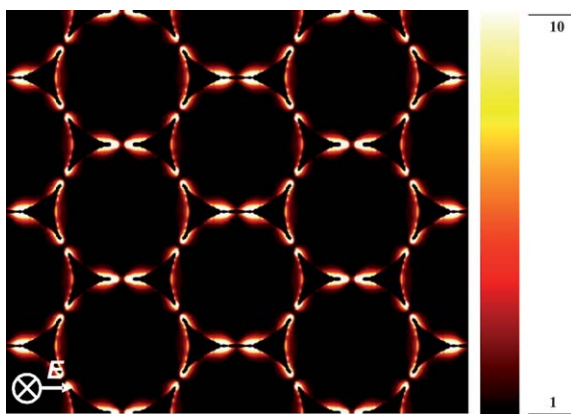


**Fig. 2** Normalized electric field energy density distribution for an array of triangular NPs arranged on a fused silica substrate. The normalization is performed with respect to the electric field energy density distribution of a fused silica substrate. The incident electric field is linearly polarized along the common bisector of the triangles. The energy density has been time-averaged on the duration of the incident pulse.

ablation threshold has been overcome (Fig. 1a). Increasing the fluence, the confinement of the light energy on the two other tips exhibiting the lowest field enhancements in Fig. 2 produce energy densities able to overcome the ablation threshold, such that besides the major hole, two minor holes are created (Fig. 1b). Finally, the generation of the most important structure, the nanogrooves, is an interplay of two effects. Firstly, due to the high applied fluence, the electric field energy densities significantly increase so that their distribution shows overlapping areas. Secondly, the energy densities of the two mainly excited tips of neighboring triangles merge together creating the ablation areas shown in Fig. 1c. Both effects lead to a nearly homogeneous ablation of material and the bone-like structures are generated. We thus have perfect agreement between the experiments and the simulations.

### B. Influence of the applied energy

As mentioned before, the pulse energy has been varied from  $E = 0.1\ \mu\text{J}$  to  $E = 7.0\ \mu\text{J}$ . However, for the same direction of the polarization of the laser light with respect to the orientation of the triangles, similar nanopatterns have been formed in regions 1 to 3, independent of the applied energy. Fig. 3a depicts a 3D-AFM image of the nanogrooves, which exhibit the same bone-like shape and almost similar dimensions as before. The nanogrooves have been generated in region 3, after irradiation with a single laser pulse with an energy of  $E = 2\ \mu\text{J}$ .

The polarization of the laser light was again almost parallel to the bisectors of the triangles. The only difference is, that the generated nanogrooves appear at larger distances from the central spot due to the higher fluence of the laser light ( $\approx 0.8\ \text{J cm}^{-2}$ ). The grooves have an average depth of  $\langle D \rangle = (11 \pm 2)\ \text{nm}$ , an average length of  $\langle L \rangle = (267 \pm 10)\ \text{nm}$ , and an average width of  $\langle W \rangle = (39 \pm 5)\ \text{nm}$ . Fig. 3b depicts a height profile of the generated nanogrooves, as indicated in Fig. 3a. It demonstrates that the generated nanogrooves have the same depth. Therefore, homogeneous ablation in the areas with high local fields occurs. In addition, the height profile reveals, that the nanogrooves are surrounded by a rim. Very likely, it is caused by surface melting, which resolidifies on the substrate at the borders of the nanostructures, as previously explained by other authors.<sup>11,12</sup>

### C. Influence of the polarization direction

To demonstrate the influence of the polarization direction, an additional set of experiments has been performed. For these experiments, the polarization direction has been rotated by  $90^\circ$  with respect to the triangular NPs. Hence, the polarization is almost parallel to a base of the triangles. The energy of the laser light was set to  $E = 3.8\ \mu\text{J}$ . Due to the high energy, the area where nanostructures are generated, coincides with the laser spot diameter of  $22\ \mu\text{m}$ . Fig. 4 depicts AFM images, which show the evolution of the nanostructures as a function

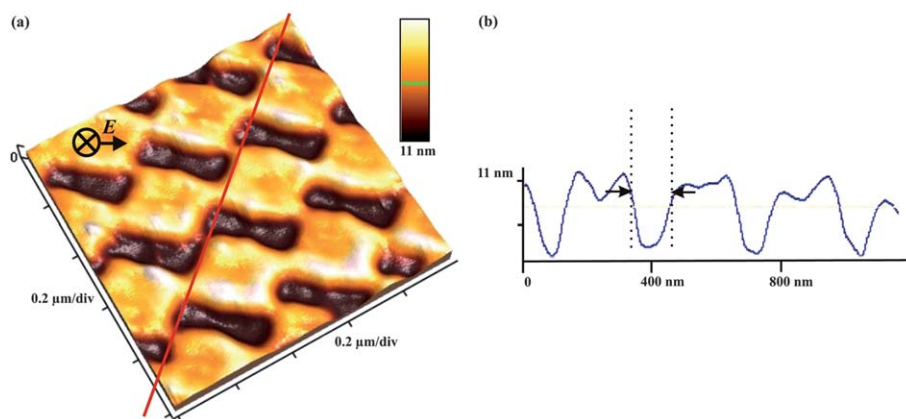


**Fig. 3** (a) 3-D AFM image of the generated nanogrooves in region 3. The applied pulse energy was set to  $E = 2 \mu\text{J}$ . The black arrow indicates the polarization direction of the incoming laser light. (b) Height profile of the generated nanogrooves, demonstrating that all the nanogrooves have the same depth.

of energy, *i.e.*, in regions 1 to 3. Again, the nanopatterns are located at the original position of the removed triangles. Minor shape variations of the nanostructures are mainly due to the pronounced Gaussian intensity distribution of the laser spot. Although the formation of the nanopattern is the same as before—higher fluences generate larger structures—the images show remarkable differences in the morphology, as compared to the nanostructures presented in section II A. Even in region 1 (see Fig. 4a) double holes are created at a single NP. These double holes merge together with increasing fluence in region 2 (Fig. 4b). For high fluences in region 3 (Fig. 4c), micrometer long nanochannels are formed. Nevertheless, the average width and depth of the nanochannels amount to only  $\langle W \rangle = (94 \pm 3) \text{ nm}$  and  $\langle D \rangle = (31 \pm 4) \text{ nm}$ , respectively, *i.e.*, well below the diffraction limit. The dimensions of all nanostructures depicted in Fig. 4 are listed in Table 2.

As already mentioned above, the morphology of the nanostructures depends on the polarization direction of the laser light with respect to the NPs. It is obvious, that the double holes are created at the two tips of the baseline, which is parallel to the polarization direction of the laser light. In contrast to the experiments described in section II A, the third tip causes nearly no ablation, even for the highest fluence. To explain the generated structures, again FDTD simulations have been performed. Fig. 5 shows the FDTD simulation where the polarization direction of light is parallel to the base line of

the triangles. The simulations easily explain the observed double holes structures in regions 1 and 2, *i.e.*, for low and medium fluences. For high fluences, again two effects occur. First, the ablation areas underneath the two strongly excited tips of a single NP overlap and the double holes merge together. Second, the ablation areas created underneath the tips of two neighboring NPs also overlap. If the overlap is sufficiently high, an almost homogeneous ablation of the substrate occurs, leading to the formation of micrometer long nanochannels. These channels exhibit homogeneous depths and their widths are well below the diffraction limit. Again, we thus have perfect agreement between experiments and simulations.

We emphasize, that the length of the nanochannels is limited only by the area in which highly ordered triangular NPs are located and by the area which is homogeneously illuminated by the laser light. It has been demonstrated, that  $6 \mu\text{m}$  long channels with an extremely homogeneous depth are easily prepared.<sup>17</sup>

#### D. Circular polarization

In order to investigate the effect of an enlarged polarization space on nanopatterning, experiments with circularly polarized light were performed. As compared to the nanostructures obtained with linearly polarized laser light, the ones obtained by circularly polarized light are more symmetric (see Fig. 6a and 6b). This can be explained as

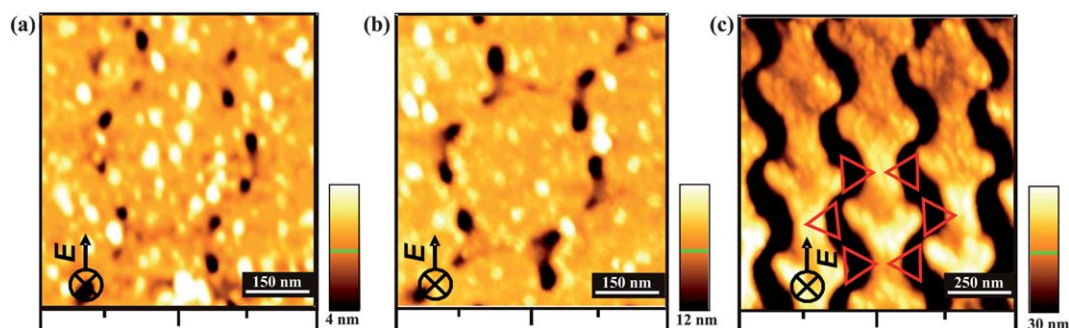


**Fig. 4** AFM image of the generated nanopatterns in region 1 (a), region 2 (b), and region 3 (c). The applied pulse energy was  $E = 3.8 \mu\text{J}$ . The red triangles indicate the original position of the triangular NPs on the substrate prior to irradiation. Again, for clarity reasons, the red triangles have been drawn larger than the original NPs, which, in fact, have a tip to tip distance of approximately  $100 \text{ nm}$ . The black arrow indicates the polarization direction of the laser light.

**Table 2** Characteristic features of the generated nanostructures for different fluences. The polarization of the applied laser light was parallel to a baseline of the triangular NPs (*cf.* Fig. 4)

| Region | Average local fluence/ $\text{J cm}^{-2}$ | Structure               | Average depth/nm | Average length/nm     | Average width/nm |
|--------|---|-------------------------|------------------|-----------------------|------------------|
| 1      | 0.38                                      | Elliptical holes        | $4 \pm 1$        | $34 \pm 4$            | $28 \pm 3$       |
| 2      | 0.70                                      | Elliptical double holes | $9 \pm 3$        | $47 \pm 5$            | $40 \pm 4$       |
| 3      | 1.73                                      | Nanochannels            | $31 \pm 4$       | several $\mu\text{m}$ | $93 \pm 3$       |

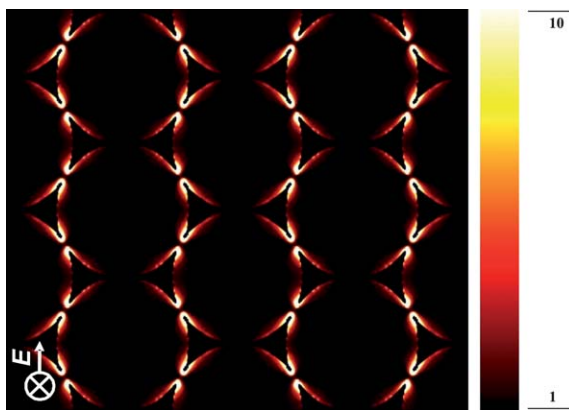


**Fig. 5** Normalized electric field energy density distribution for an array of triangular NPs arranged on a fused silica substrate. The normalization is performed with respect to the electric field energy density distribution of a fused silica substrate. The incident electric field, is linearly polarized along a base of the triangles. The energy density has been time-averaged on the duration of the incident pulse.

follows: circularly polarized light is nothing more than a linearly polarized light rotating at the optical frequency of interest. The light pulse launched on the sample has a finite temporal width (35 fs). As compared to the optical frequency of interest (a wavelength of 790 nm corresponds to a frequency of 0.38 PetaHertz), the polarization direction of the light crossing the interface between the fused silica substrate and the gold triangles has time to rotate more than 12 cycles during the pulse duration. The ablation process thus results from the averaging of the linear polarization over many rotations, leading to the observation of a more symmetric pattern in Fig. 6a and 6b. The same high symmetry pattern has been obtained in our simulations (Fig. 6c), by averaging the electric field energy density on the time scale of the pulse duration. The differences exhibited between the simulated (perfect) pattern and experimentally obtained pattern can be easily explained with the fact that the triangular NPs observed experimentally may present different kinds of imperfections such as

a slight disorder intrinsically due to the deposition procedure. Such imperfections are random in nature and so are not taken into account in the simulations. They are more clearly revealed in circular polarization with respect to the linear polarizations previously investigated as a result of the broader configuration space explored.

### III. Conclusions

In this paper we have demonstrated a simple method for designing and tuning nanopatterns on fused silica substrates exploiting the polarization dependence of the strongly localized near field of highly ordered triangular NP arrays. To generate strong enough near fields, the samples were irradiated with single 35 fs laser pulses. Although the average fluence was significantly below the ablation threshold of the fused silica substrates, ablation occurs in the vicinity of the triangular NPs due to enhanced near fields. Since these near fields are strongly localized, the ablation threshold can be overcome in tiny areas, leading to nanostructures well below the diffraction limit. Different nanostructures have been created, depending on applied fluence and the polarization direction of the laser light with respect to the NP orientation on the substrate. Besides hole structures, nanogrooves and micrometer long nanochannels, all with lateral dimensions well below the diffraction limit, have been generated. FDTD simulations perfectly explain the different obtained nanostructures due to strong local fields, which are driven by the excitation of plasmon resonances in the triangular NPs. Bone-like nanogrooves in a chequered structure are obtained for a polarization direction of the incoming laser light parallel to the bisector of two neighboring triangles. Nanochannels are generated, if the polarization is parallel to a base of the triangular NPs. In particular, the generated nanogrooves and nanochannels open up a new dimension for applications in modern nanotechnology.

R.M and P.D acknowledge financial support from the EU-FEDER and Interreg IV, project "PlasmoBio". B.K acknowledges financial support from Smart film grant 830039 (ECV12020020892F) in the framework of Convergence Project. R.M, P.D, B.K and R.A.L.V acknowledge financial support of F.N.

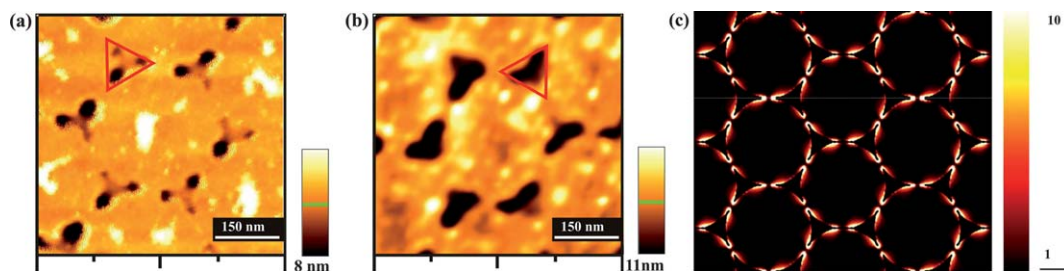


**Fig. 6** AFM images of the generated nanopatterns after applying a single fs light pulse with an average fluence of  $F \approx 0.072 \text{ J cm}^{-2}$  (a) and  $F \approx 0.7 \text{ J cm}^{-2}$  (b) using circular polarized light. (c) Normalized electric-field energy density distribution for an array of triangular NPs arranged on a fused silica substrate where the incident electric field is circularly polarized.

R.S. F.H and F.T acknowledge project European Commission under Contract No. MRTN-CT-2003-504233. L.E and T.B acknowledge financial support by DFG.

## References

- 1 J. M. Perry, K. M. Zhou, Z. D. Harms and S. C. Jacobson, *ACS Nano*, 2010, **4**, 3897.
- 2 S. M. Xiao, V. P. Drachev, A. V. Kildishev, X. Ni, U. K. Chettiar, H. K. Yuan and V. M. Shalaev, *Nature*, 2010, **466**, 735.
- 3 G. R. Hendrickson, M. H. Smith, A. B. South and L. A. Lyon, *Adv. Funct. Mater.*, 2010, **20**, 1697.
- 4 N. Tate, H. Tokoro, K. Takeda, W. Nomura, T. Yatsui, T. Kawazoe, M. Naruse, S.-I. Ohkoshi and M. Ohtsu, *Appl. Phys. B: Lasers Opt.*, 2010, **98**, 685.
- 5 Y. F. Lu, Z. H. Mai, G. Qiu and W. K. Chim, *Appl. Phys. Lett.*, 1999, **75**, 2359.
- 6 Y. Lu and S. C. Chen, *Nanotechnology*, 2003, **14**, 505.
- 7 W. Cai and R. Piestun, *Appl. Phys. Lett.*, 2006, **88**, 111112.
- 8 H. J. Münzer, M. Mosbacher, M. Bertsch, J. Zimmermann, P. Leiderer and J. Boneberg, *J. Microsc.*, 2001, **202**, 129.
- 9 M. Mosbacher, H. J. Münzer, J. Zimmermann, J. Solis, J. Boneberg and P. Leiderer, *Appl. Phys. A: Mater. Sci. Process.*, 2001, **72**, 41.
- 10 D. Brodoceanu, L. Landström and D. Bäuerle, *Appl. Phys. A: Mater. Sci. Process.*, 2007, **86**, 313.
- 11 D. Eversole, B. Luk'yanchuk and A. Ben-Yakar, *Appl. Phys. A: Mater. Sci. Process.*, 2007, **89**, 283.
- 12 P. Leiderer, C. Bartels, J. König-Birk, M. Mosbacher and J. Boneberg, *Appl. Phys. Lett.*, 2004, **85**, 5370.
- 13 N. N. Nedyalkov, T. Miyanishi and M. Obara, *Appl. Surf. Sci.*, 2007, **253**, 6558.
- 14 N. N. Nedyalkov, T. Sakai, T. Miyanishi and M. Obara, *Appl. Phys. Lett.*, 2007, **90**, 123106.
- 15 A. Heltzel, S. Theppakuttai, S. C. Chen and J. Howell, *Nanotechnology*, 2008, **19**, 025305.
- 16 R. K. Harrison and A. Ben-Yakar, *Opt. Express*, 2010, **18**, 22556.
- 17 F. Hubenthal, R. Morarescu, L. Englert, L. Haag, T. Baumert and F. Träger, *Appl. Phys. Lett.*, 2009, **95**, 063101.
- 18 N. Gupta, B. F. Lin, L. Campos, M. D. Dimitriou, S. T. Hikita, N. D. Treat, M. V. Tirrell, D. O. Clegg, E. J. Kramer and C. J. Hawker, *Nat. Chem.*, 2010, **2**, 138.
- 19 A. V. Krasavin and A. V. Zayats, *Appl. Phys. Lett.*, 2010, **97**, 041107.
- 20 J. C. Hulteen, D. A. Treichel, M. T. Smith, M. L. Duval, T. R. Jensen and R. P. V. Duyne, *J. Phys. Chem. B*, 1999, **103**, 3854.
- 21 R. Micheletto, H. Fukuda and M. Ohtsu, *Langmuir*, 1995, **11**, 3333.
- 22 L. J. Sherry, R. Jin, C. A. Mirkin, G. C. Schatz and R. P. V. Duyne, *Nano Lett.*, 2006, **6**, 2060.
- 23 K. L. Shuford, M. A. Ratner and G. C. Schatz, *J. Chem. Phys.*, 2005, **123**, 114713.
- 24 J. E. Millstone, S. Park, K. L. Shuford, L. Qin, G. C. Schatz and C. A. Mirkin, *J. Am. Chem. Soc.*, 2005, **127**, 5312.
- 25 L. Englert, B. Rethfeld, L. Haag, M. Wollenhaupt, C. Sarpe-Tudoran and T. Baumert, *Opt. Express*, 2007, **15**, 17855.
- 26 M. Lenzner, J. Krüger, S. Sartania, Z. Cheng, C. Spielmann, G. Mourou, W. Kautek and F. Krausz, *Phys. Rev. Lett.*, 1998, **80**, 4076.